Visualization of hydraulic conditions inside the feed channel of Reverse Osmosis
A practical comparison of velocity between empty and spacer-filled channel

Haidari, A. H.; Heijman, S. G J; van der Meer, W. G J

DOI
10.1016/j.watres.2016.10.012

Publication date
2016

Document Version
Accepted author manuscript

Published in
Water Research

Visualization of hydraulic conditions inside the feed channel of Reverse Osmosis

A practical comparison of velocity between empty and spacer-filled channel

A.H. Haidari[a1], S.G.J. Heijman[a], W.G.J. van der Meer[a,b]

a: Delft University of Technology, Department of Civil Engineering, Stevinweg 01, 2628 CN Delft, The Netherlands

b: Oasen NV, P.O. Box 122, 2800 AC Gouda, the Netherlands

Abstract

It is widely accepted that our understanding about the membrane process increases by investigation of the hydraulic conditions of membranes. While numerical studies have been broadly used for this purpose, the experimental studies of a comparable resolution are scarce. In this study, we compared the pressure drop, the temporal and the spatial velocity maps of a spacer-filled channel and an empty channel of the same size to determine the effect of presence of the feeds spacer on hydraulic conditions. The velocity maps are obtained experimentally by using of the Particle Image Velocimetry (PIV) technique. Application of the feed spacer caused 2-8.5 higher pressure drop increase in the experimental conditions in this research. The flow had a spatial distribution in the form of a unimodal symmetric curve of normal distribution in the empty channel and a bimodal asymmetric curve in the spacer-filled channel. The bimodal curve indicates the presence of high- and low-velocity zones.

[1] Corresponding author at: Room S3.02.020, Stevinweg 01 (Building 23 = Civil Engineering faculty of Delft university of technology), 2628CN Delft, The Netherlands.

Tel.: +31 17 2787337

E-mail address: a.h.haidari@tudelft.nl (A.H Haidari)

Additionally, the low-velocity zones showed also a lower variation of velocity in time, which indicates the high fouling potential of these locations. The results from this study may be uses for validation of numerical studies.

Keywords: Feed spacer, Membrane, Particle Image Velocimetry, Reverse Osmosis, Spiral Wound Modules

Introduction

Application of Reverse Osmosis (RO) for purification of water increases continuously. Spiral Wound (SW) modules of RO (RO) are the most applied configuration in drinking and wastewater. The feed spacer as one of the main parts of the SW modules of RO plays an important role in hydrodynamic inside these modules. The feed spacer acts as a stabilizer by separating the membranes' leaves and forming of the feed channel. Alternatively, it disrupts the flow and enhances the flow mixing between the bulk of the fluid and the fluid adjacent to the membrane surface. The latter improves the mass transfer, albeit at the expense of increases in energy losses (Da Costa and Fane 1994, Zimmerer and Kottke 1996). The benefits of mass transfer enhancement often outweigh the disadvantages caused by increased energy losses such that it becomes more economically attractive to operate membrane systems with spacer than without (Da Costa et al. 1991, Fimbres-Weihs and Wiley 2010, Thomas et al. 1970). The former studies have shown that current feed spacer could themselves become a source of fouling, particularly biofouling (Araùjo et al. 2012, Vrouwenvelder et al. 2007, Vrouwenvelder et al. 2010a, Vrouwenvelder et al. 2003, Vrouwenvelder et al. 2008, Vrouwenvelder and Van Der Kooij 2003, Vrouwenvelder et al. 2011, Vrouwenvelder et al. 2009, Vrouwenvelder et al. 2006). The biofouling becomes more highlighted in surface freshwater or municipal wastewater than the saline water resources because of the lower potential of freshwater for creation of the concentration polarization. Therefore, design of feed spacers to promote the flow instabilities simultaneously with minimizing of energy losses and fouling will contribute enormously to improvement of a membrane's configuration. The design of an optimal feed spacer requires a deep understanding of the flow conditions through studying the flow velocity map, deceleration locations and flow distributions in the feed channel. This can be done experimentally or by using of computational simulation.

Computational techniques provide high-resolution velocity maps and have relatively lower costs and risks compare to experimental methods. However, application of these numerical techniques may be associated with difficulties such as matching of exact geometry of the modeled-spacer with reality,

simulation of fouling, and accurate verification and validation of these models. Many numerical studies are done with simplified spacer geometry, while geometrical details of the filaments in the feed spacer have remarkable effects on the hydrodynamics of channel and the fouling. For instance, Neal *et al.* (Neal et al. 2003) showed experimentally that particle deposition occurs around the point where the attached filaments to membrane bulge outward. While advances in the technology such as the 3D-printing provide a promising solution to this difficulty, the fouling process, as one of the main phenomena taking place in membrane systems, remains as a complicated and time consuming part to be incorporated into numerical models (Fimbres-Weihs and Wiley 2010). According to Fimbres and Wiley (Fimbres-Weihs and Wiley 2010), and Schausberger *et al.* (Schausberger et al. 2009), the fouling models that are developed before them (Schausberger et al. 2009, Schwinge et al. 2002, Yee et al. 2009) could not be used as a reliable predictive design tool. As mentioned by former studies (Fimbres-Weihs and Wiley 2010, Oberkampf and Trucano 2002), the verification deals with mathematics of the model, while validation deals with its physics. Oberkampf and Trucano referred in their study (Oberkampf and Trucano 2002) to the five most common sources of the numerical errors that could be present within a model. These numerical errors result is defining a different set of equations than the system of partial differential equations, that the transport equations defined, and consequently, not accurate verification of the model (Fimbres-Weihs and Wiley 2010). Validation is one of the main difficulties that most computational studies within the field of membrane science face. Therefore, some researchers (Fimbres-Weihs and Wiley 2010, Willems et al. 2010) recommended applying of direct, non-invasive, high resolution experimental methods such as the Particle Image Velocimetry (PIV).

To authors' knowledge, PIV is used only by Gimmelshtein and Semiat(Gimmelshtein and Semiat 2005), and Willems *et al.* (Willems et al. 2010) for flow investigation inside the SW modules of RO. Gimmelstein and Semiat (Gimmelshtein and Semiat 2005)studied the liquid flow in spacer-filled cells in the velocity ranges from 0.06-1.3 m/s. Willems *et al.* (Willems et al. 2010) investigated the liquid velocity profiles of water and water-air mixture in spacer-filled channels. Gimmelstein en Semiat

(Gimmelshtein and Semiat 2005)showed that the bulk of fluid flows in a straight line from inlet to outlet with only small deviations near the filaments. Willems *et al.* (Willems et al. 2010) found that liquid flows mainly parallel to the spacers' filaments and therefore, the direction of flow changed 90^{o} over the height of the channel. Willems *et al.* (Willems et al. 2010) related the disagreement of their findings with those of Gimmelshtein and Semiat (Gimmelshtein and Semiat 2005) to that in their setup the spacer filled the whole height of channel whereas in the study of Gemmelshtein and Semiat 20% of the height of the feed channel was empty. Willem *et al.* (Willems et al. 2010) found that the liquid velocity was unsteady in one phase and two phase flow, which was in agreement with different studies (Koutsou et al. 2007, Lau et al. 2009, Li et al. 2002, 2005) done with CFD.

Because of the limited availability of PIV-studies in the spacer-filled of RO and the empty channel (slit) of the same size, we studied the flow of water through the empty and spacer-filled channel at Reynolds' numbers (Re) below 250 to provide a visual aid for a better understanding of the flow inside SW modules of RO. To this end, first the terms that are used throughout this paper are explained and then the setup and measurement methods are described. After that, the effects of introducing of a typical feed spacer of RO to an empty feed channel on the pressure drop are investigated. In the next section, the temporal velocity acquired from the PIV measurement is studied as these types of information are scares in literature. After that, the spatial velocity is measured, and the results are compared to the available experimental data and the CFD studies. Finally, the effect of increase of Reynolds number on velocity pattern inside the spacer-filled channel is studied.

Experimental

The current study involved measuring of the flow and pressure drop for the calculation of friction losses and visualization of velocity. The experiments were performed with the setup depicted in Figure 1, which consists of a magnetic stirrer (01), solution of suspended fluorescent particles (02), a feed pump (03), a mass-flow meter (04), a flow cell (05), a differential pressure transmitter (06), a PC for registration of mass-flow values (07), and the PIV-system (08-11).

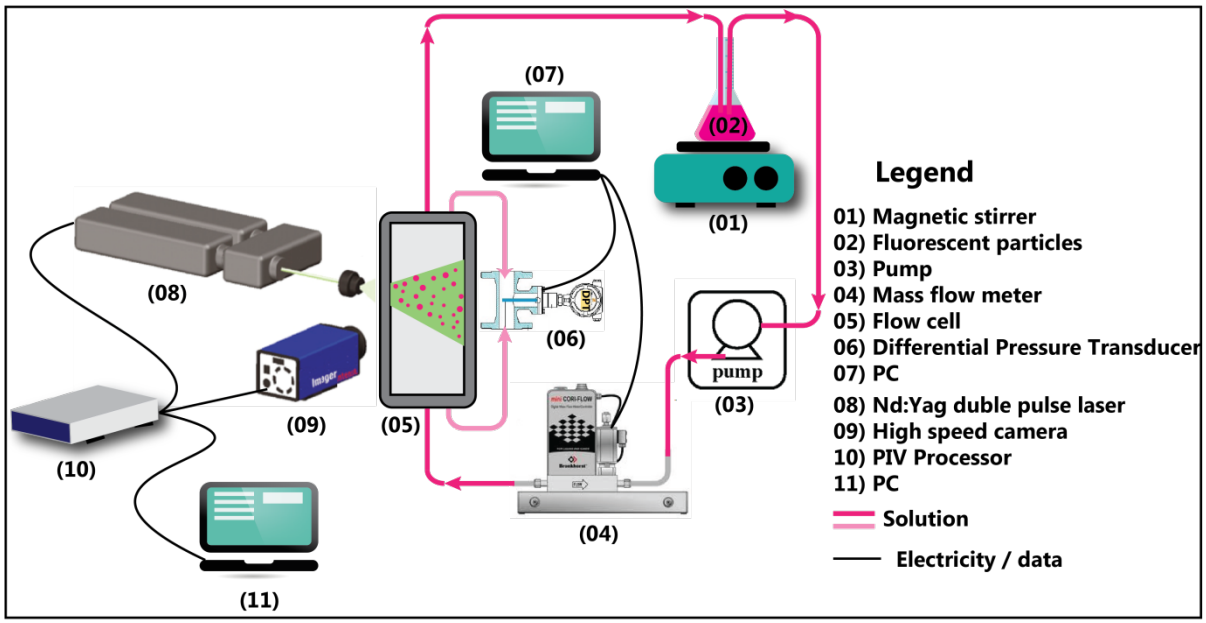

Figure 1: Experimental setup. The setup can be divided into two parts. Par A is mainly used for measurement of the flow, density and temperature, which are used for calculation of average velocity and friction losses. Part B is mainly used for visualization of the flow and velocity inside the feed channel.

The solution, which contains the suspended fluorescent particles (Dantec, Ulm, Germany), is pumped through the mass-flow meter (Bronkhorst Instruments, Ruurlo, The Netherlands) into the flow cell (Demo, Delft, The Netherlands) over which the differential pressure is measured by means of a differential pressure transmitter (Endress+Hauser, Naarden, The Netherlands). The mass flow meter registers the flow, solution density, and temperature. The mass flow meter and differential pressure transmitter have respectively an accuracy of 0.2% and 0.075% for liquids. The particles have a mean volume-distribution size of 10µm, a density of 1.19g/cm^3 and are coated with Rhodamine-B. The

coated particles were used in combination with a cutoff filter (Lavision, Grove, UK) to improve the quality of the vector maps. The cutoff filter centered around the emission wave length of the particles (ʎ=545nm) and therefore, allows only the emitted fluorescent light from the tracer particles to pass. Accordingly, the high background light level, as the consequence of application of the spacer and membrane, is reduced and the quality of the vector maps is improved. The flow cell was operated without permeation because the permeate-flow in RO is small compare to cross-flow velocity. The membrane coupon and the spacer are located in the flow channel (L= 200mm, W= 40mm and H=0.7mm) embedded in the flow cell (L=260mm, W=85mm, H=55mm). In contrary to the spacer-filled channel experiments in which the total height of the flow channel was filled with the membrane and spacer, the empty channel experiments were carried out with only the membrane coupon (Trisep-AMC1) inside the feed channel. Each experiment was carried out at different flow rates and a constant temperature (<0.8% maximum error from the average temperature). However, the same flow rates were applied in the empty and spacer-filled channel, which resulted in different theoretical average velocity. The average velocity, which also known as the effective velocity in some literatures (Fimbres-Weihs and Wiley 2007, Fimbres-Weihs and Wiley 2010), is calculated by dividing the velocity of empty channel (superficial velocity) to the porosity of the feed spacer.

$$U_{ave}(U_{eff}) = \frac{U_{sup}}{\varepsilon} = \frac{Q}{A_{eff}} = \frac{Q}{A.\varepsilon} = \frac{Q}{W.H.\varepsilon} \qquad \text{Equation 1}$$

In this study, a nonwoven commercial polypropylene (PP) spacer was used of which the geometric data are summarized in Table 1. The porosity of the spacer and the hydraulic diameter of the feed channel are respectively calculated by using Equation 3 (Da Costa et al. 1994) and Equation 3 (Da Costa et al. 1994, Fimbres-Weihs and Wiley 2010)

$$\varepsilon = 1 - \frac{\pi d_f^2}{2 l_m h_{sp} \sin\theta} \qquad \text{Equation 2}$$

$$d_h = \frac{4 \times \varepsilon}{\frac{2}{H} + (1 - \varepsilon)\, S_{v,SP}}$$ Equation 3

Table 1: the specification of empty channel (empty channel) and spacer-filled channel

Id	Channel height (spacer's thickness)	Filament length	Filament angle	Porosity	Hydraulic diameter	Material
Unit	(mm)	(mm)	(°)	(%)	(mm)	(-)
Empty channel (Slit)	0.76mm	NA	NA	100	1.50	Without spacer
Spacer-filled channel	0.76mm	2.33	89.5	87	0.88	polypropylene

For the calculation of average velocity, it was assumed that the thickness of a filament is the same over its length in a mesh while, in reality, the thickness of a manufactured-filament varies over its length. It is also assumed that the channel height is twice as high as a filament while it is slightly smaller because at nodes, at which the spacer's thickness and feed channel's height is determined, the top and bottom filaments are slightly embedded in each other (Figure 2).

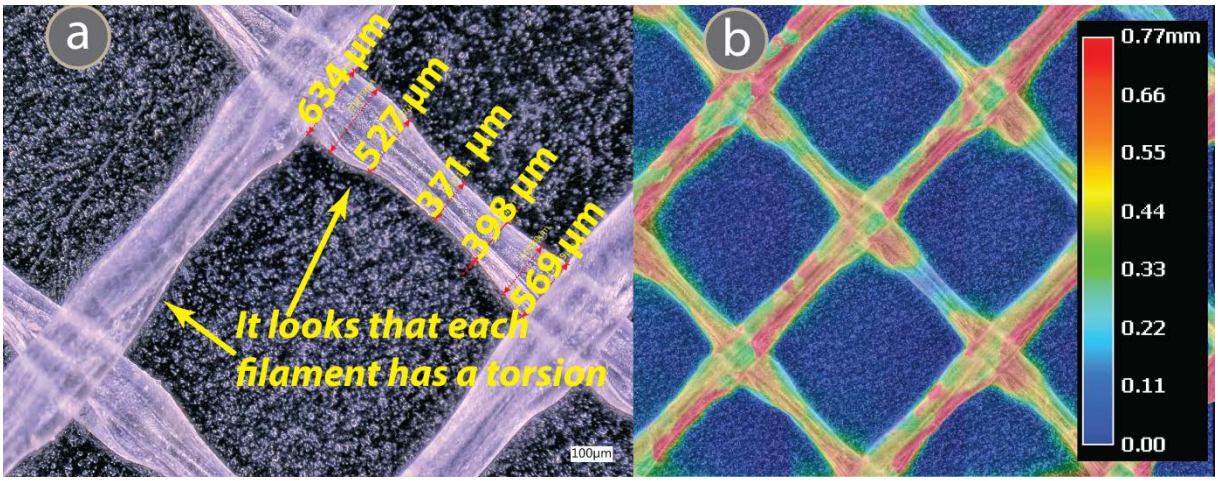

Figure 2: The typical commercial feed spacer (non-woven and 30mil (0.76mm) thick). Image "a" shows dimensions of a filament. Image "b" shows the position of the spacer with respect to the membrane surface. The figure shows an uneven filaments' cross-section over their length. Also a slight torsion is visible in each filament. These types of geometrical details are normally not incorporated in the computational models.

During the PIV-measurements, the fluorescent particles inside the channel are illuminated by a laser (Nano S, Nd:Yag laser, Litron laser, UK) with two light-pulses of a short interval. A high-speed camera (Lavision, Grove, UK) is recorded two frames exposed by the laser light-pulses. The time interval between two pulses (two frames) was adjusted to the particles-displacement in order to reduce the

number of pairing losses (loss of particle images within the interrogation window from the first frame to the second frame). The time interval was varied from 150-2500µs depending on the flow rate inside the channel and presence of the spacer. Each of the captured frames is divided into small interrogation areas. An embedded algorithm in the software determines the shift of intensity pattern in each of these small areas. The controlled time interval and calculated displacement are used for calculation of the velocity vectors. In order to limit the effects of boundaries (entrance, edges and exit) on the flow and to ensure a fully developed flow, the frames are taken at about 100mm from the inlet and 15mm from each edge of the cell.

The PIV-images were captured at three different heights in the feed channel separately: close to the camera (Z3), middle of the channel (Z2) and far from the camera or close to membrane sheet at the bottom of the feed channel (Z1) (Figure 3). Since the thickness of the laser sheet light (2 mm) is greater than the thickness of feed channel (0.7mm) the whole height of the channel is therefore illuminated. That is a common situation in µPIV (Willems et al. 2010) which is solved by fixing the camera focus at a specific distance from the lens and moving the object (Klank et al. 2002, Willems et al. 2010). In this study, the camera focus was fixed as a specific distance from lens and the camera is moved on the translation stage, because moving of the object was not possible. The translation stage made it possible to move the camera 50µm in each step. The camera was initially placed such that particles in the middle of the channel and close to membrane were barely in focus (Z3). Then the camera is moved to the next positions (Z1, Z2) with translating stage. The depth of field of the setup was about 0.14mm.

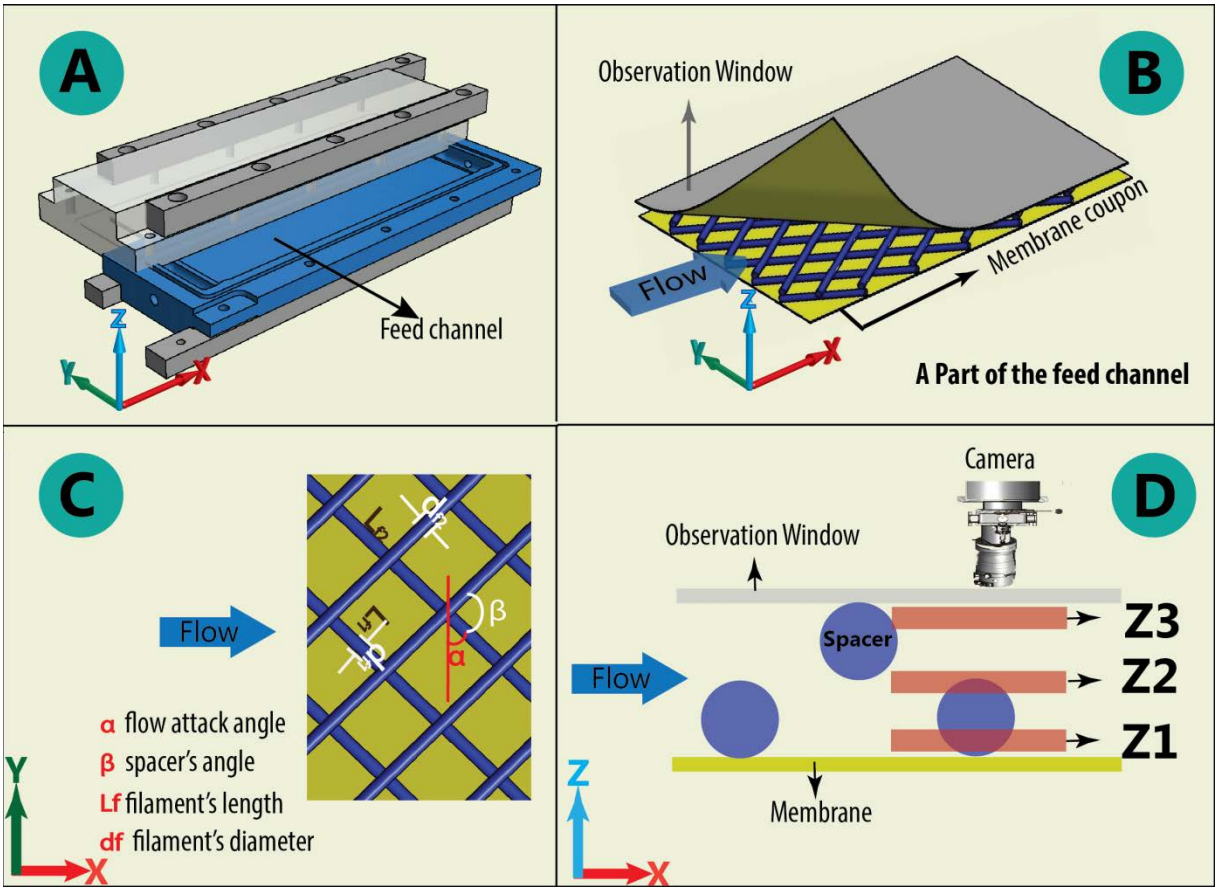

Figure 3: The flow cell (L=260mm, W=85mm, H=55mm) is made of a Plexiglas at top, which serves as an observation window. The flow channel (L= 200mm, W=40mm, H=0.7mm) is embedded in the bottom part of the flow cell (A). A membrane coupon and the feed spacer are placed in the feed channel under the observation window (B). Definition of the spacer nomenclature used in this study (C). Definition of the focusing depth of the camera (D)

For each specific flow rate and depth, 50 pairs of images (100 frames) were taken (Figure 4a) with the time interval of about 30mS. A momentary velocity map is calculated for each pair of frames, which is resulted in 50 instantaneous velocity maps (Figure 4b). These 50 images are used to compare the temporal velocity inside the feed channels. An average of these 50 pictures (Figure 4C) is used to study the spatial velocity inside the feed channel.

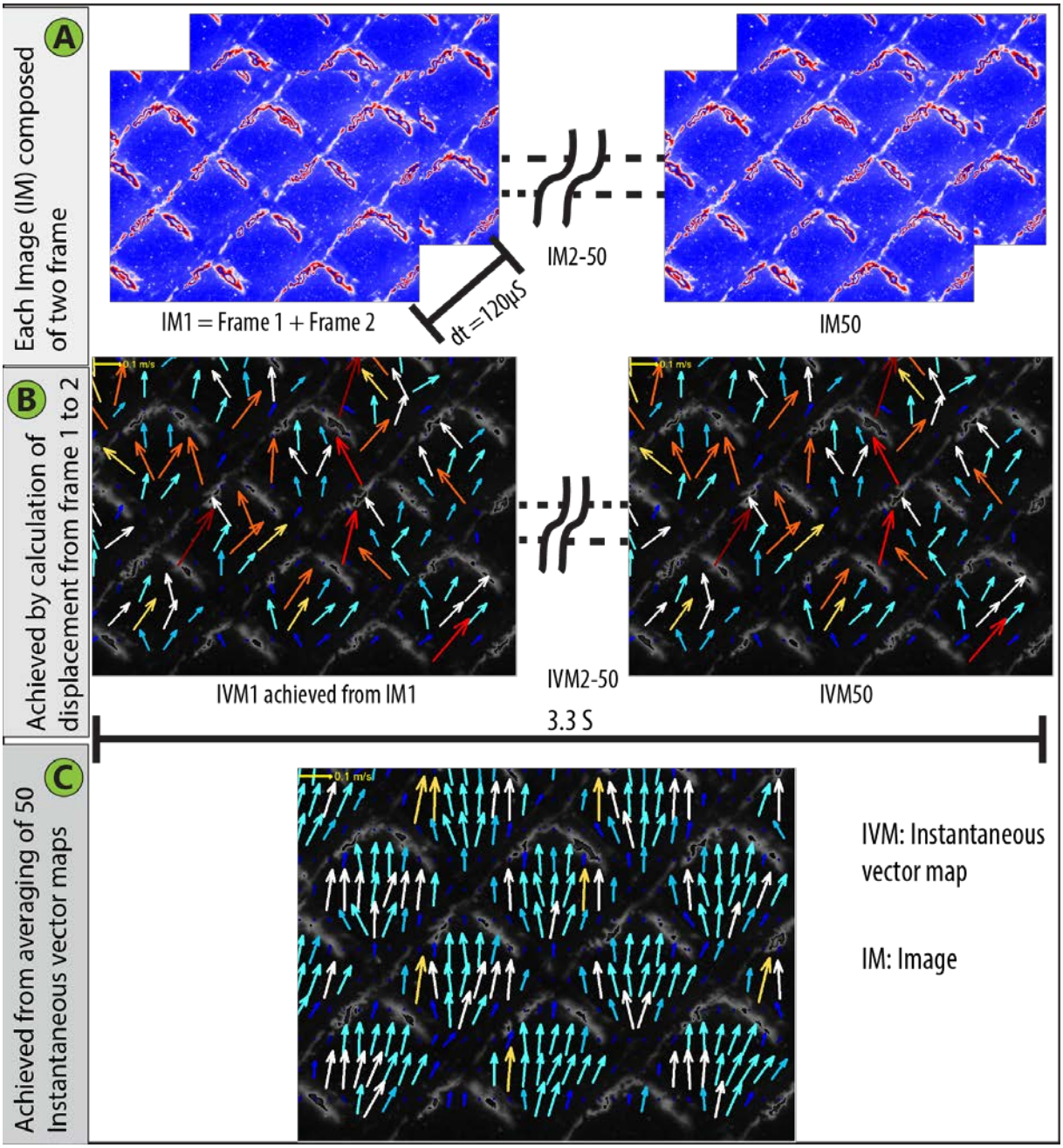

Figure 4: PIV measurement and data analysis: 50 pairs of images are taken, with a time interval of 120 μs between two frames of each pair of pictures and time interval of 0.06s between each pair (a). Using each pair picture, the instantaneous velocity of the respective pair is calculated (b). Average of all 50 velocity maps is presented as the average velocity(c).

Results

Pressure drop

The driving force of SW modules of RO critically affects by the pressure losses in the feed channel which increase using of the feed spacer (Da Costa et al. 1994, Schock and Miquel 1987, Zimmerer and Kottke 1996). The pressure drop of a spacer-filled channel depends on the viscous drag on the spacer, the form drag, the kinetic losses or eddies due to directional flow changes, and the viscous drag on the channel walls (Da Costa et al. 1994). All of these components are related directly or indirectly to the average velocity in direction of the flow (U_x) albeit with different magnitude. The flow condition (if a flow is laminar or not) is determined by defining the relation between the pressure drop and the power of average velocity "m" (Equation 4). Da Costa *et al.* (Da Costa et al. 1991) suggested that for laminar flow "m" should be around one and for turbulent around 1.75. However, in turbulent flow the Reynold's number (Re) is far above the Re in the SW modules of RO. Therefore, as it has been suggested (Fimbres-Weihs and Wiley 2010, Pellerin et al. 1995), it is better to talk about the disturbance inside the flow as eddies rather than turbulence.

$$dp \propto u^m \qquad \text{Equation 4}$$

Figure 5 shows the effects of the increase in the flow rate (A) and the average velocity (B) on the pressure drop per unit length of channel. The pressure drop measured here is the total pressure drop, which consists of the pressure drop as the consequence of connecting the tubes to the pressure transducer, pressure drop at the boundary layers, and pressure drop due to the presence of the feed spacer. The pressure drop in the spacer-filled channel was (0.27 bars/m for an average velocity of 0.16 m/s) in the expected practical range of a single SW module of RO (0.2-0.3 bars/m for an average velocity of 0.16 m/s). The effect of only the feed spacer on the pressure drop is calculated by subtracting the pressure drop of the empty channel from the spacer-filled channel. This difference

was respectively 0.008 and 0.31bar/m for the lowest and highest flow rate applied. The power "m" was increased from 1.63 to 1.74 by considering only the spacer.

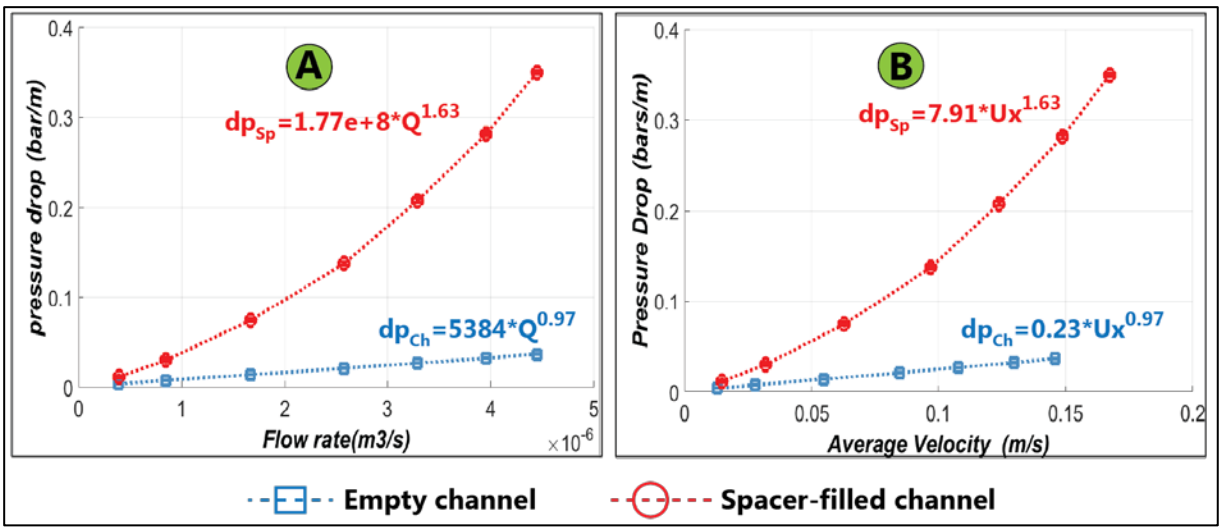

Figure 5: effects of the increase of flow and average velocity on the pressure drop in the empty and spacer-filled channel of the same height 0.762mm (30mils). The errors for flow rates (average velocity) and pressure drop are plotted in the direction of their corresponding axes and were very low to be visualized on this picture.

PIV measurements

Spatial velocity pattern

Figure 6 illustrates the spatial average velocity of the spacer-filled channel at different levels; close to the membrane (Z1), at the boundary of the top and bottom filaments (Z2) and close to the observation window of the flow channel (Z3). The measurements of each level were performed at a different momentum but with the same inlet velocity. The flow was aligned with the direction of the filaments at Z1 (close to the membrane) and Z3 (close to window). The flow at Z2 (middle of the channel) had a pattern such as the mixed image of the flow at Z1 and Z3. These results were in accordance with the results achieved by the Willems *et al.*(Willems et al. 2010) for a single-phase flow in the spacer-filled channel. The flow pattern at the middle of the channel was the same as the flow pattern observed by Lau *et al.* (Lau et al. 2009) when they used a spacer of 1.0mm thick with a

flow attack angle of 45° and a Re of 600 (fig. 07 in their work). However, the length of filament is not mentioned in the provided literature.

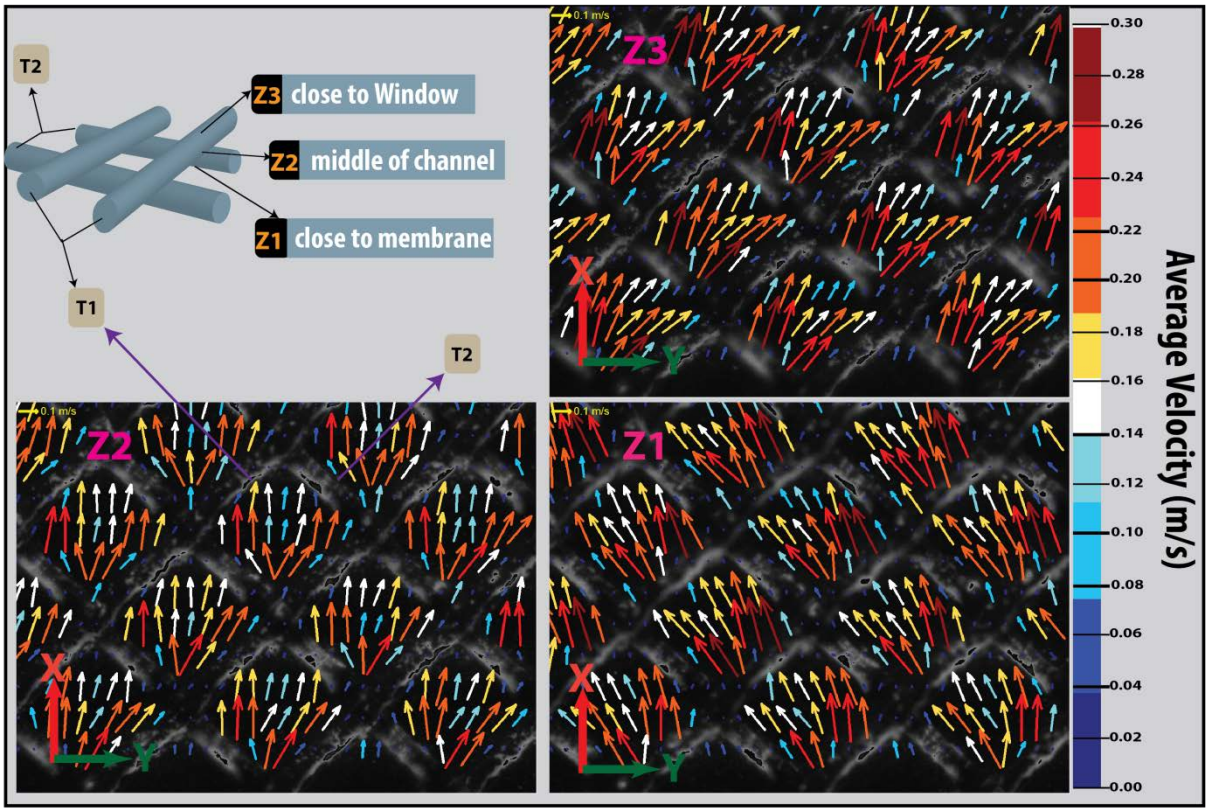

Figure 6: spatial variations of the velocity averaged over time for the spacer-filled channel at different levels; close to the membrane (Z1), at the middle of the channel (Z2), and close to the observation window (Z3). The inlet velocity used here was 0.17m/s.

While, the presented results in Figure 6 correspond to the highest average velocity only, the flow patterns remained the same by decreasing of the average velocity to 0.06m/s (Figure 7). However, by further decrease of the velocity, the flow pattern deviated more from the flow pattern shown in Figure 6 particularly at Z1 and Z3 planes. In these low flow conditions, the flow pattern was not aligned in the direction of the filaments anymore but in the direction of the flow from the inlet to outlet in a straight line albeit with some deviations close to the filaments.

As expected, the flow in the empty channel was in the straight line from the inlet to the outlet (the results are not shown here). In the conditions with an average velocity lower than 0.04m/s, however,

the flow was slightly deviated from the straight line patterns especially at the Z1 and Z3 planes. The average velocity in empty and spacer-filled channel was deviated from the measured velocity. This difference is the results of measuring the fully developed flow velocity at the middle of the channel, while introducing the inlet velocity as the average velocity by the Equation 1. The fully developed velocity has a parabolic shape in the Z direction with the lowest velocity at Z1 and Z3 and the highest velocity at Z2. The entrance length, which is defined as the length of the channel that the flow becomes fully developed, is about 2.17cm for a rectangular channel with an aspect ratio of 1/50 (H/W) (Du Plessis and Collins 1992).

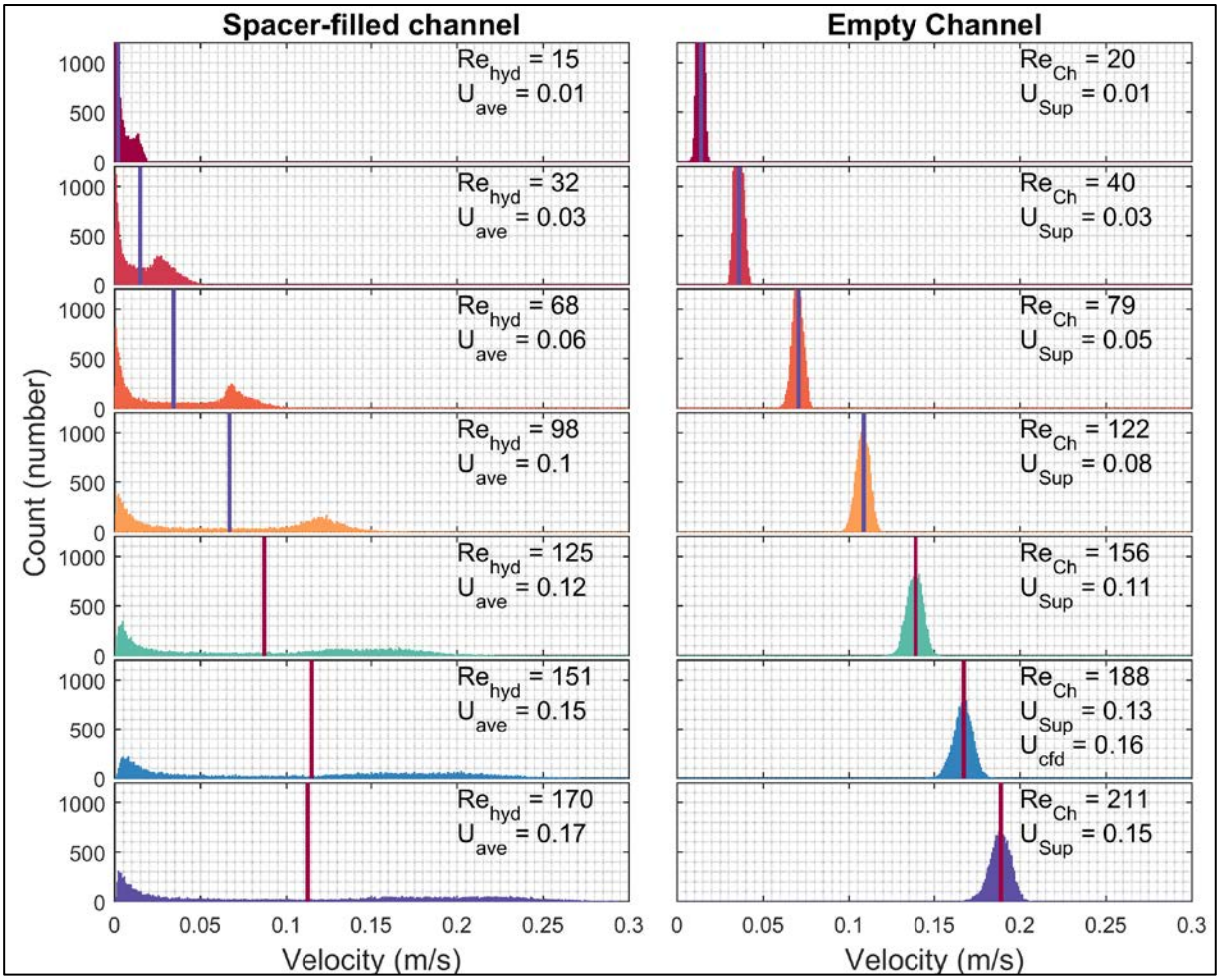

Figure 7: development of velocity inside the empty channel and the spacer-filled channel. The vertical line indicates the median of the data. The measured velocity is shown on the x-axis and the number of corresponded particles on the y-axis. By the increase of flow, the average velocity increases but the velocity patterns remain the same.

Figure 8 illustrates the velocity pattern with an average inlet velocity of 0.1m/s for the field of view (left) and a magnification of a mesh (right). The results show that when the camera is focused on Z1-plane, the highest velocity occurs when the fluid passes over a filament, enter the mesh, and passes under the filament at shortest distance to exit the mesh. When the camera is focused on the Z3-plane, the highest velocity occurs when the fluid passes under a filament, enter the mesh, and passes over a filament at the shortest distance to exit the mesh. The lowest velocity can be observed at the upstream corner of each mesh (Figure 8). The pattern described here is in agreement with the velocity map shown by Bucs *et al.*(Bucs et al. 2014) (fig. 03C; in their work). The velocity pattern can be directly related to the fouling. For instance, the places with highest fouling potential can be identified by knowing the lowest velocity regions. An example of such relation can be observed by comparing of the velocity patterns showed in Figure 8 with the deposition patterns of the particles which are observed by Radu *et al.* (Radu et al. 2014). The locations of lowest velocity pattern in our study were in agreement with the deposition locations of microsphere particles when Radu *et al.* used the same orientation as in our study.

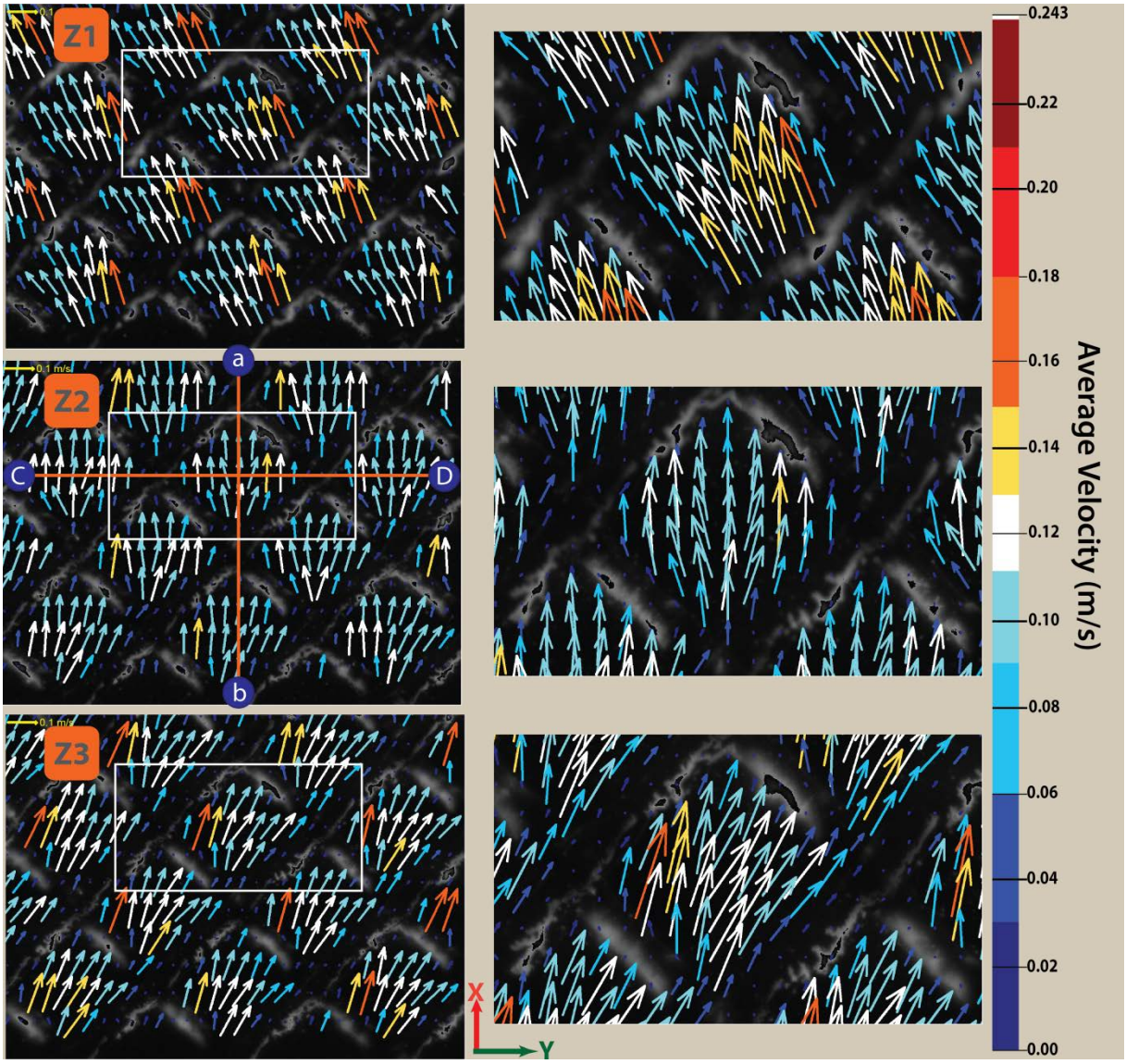

Figure 8: The pictures on the left show total field of view for three levels (Z1, Z2, and Z3) and the pictures on the right-side illustrate the zooming panel for one mesh. The velocity patterns shown here are for an average inlet velocity of 0.1m/s. The velocity profiles along lines a-b and C-D are shown in Figure 9.

Figure 9 shows the normalized velocity profile (U/U_{Slit}) over the section a-b (parallel to flow) and C-D (perpendicular to flow) at the three different levels. The velocity pattern at Z1 mirrors the pattern of Z3 along the line C-D. The velocity pattern along the C-D line at Z2 (middle of the channel) is such as the mixed pattern of Z1 and Z3.

The velocity along the line a-b has the same patterns in all three levels indicating that the flow patterns between two nodes along the flow remain the same irrespective to the height of the

measurement. It is obvious that a slight shifting of these lines results in another velocity pattern. For instance at a distance of about 25% from each node toward the middle of a mesh, the velocity pattern along a-b in Z1 mirrors the velocity pattern of Z3 while the velocity pattern along C-D remains the same as the patterns of Figure 9 (graphs are not shown here).

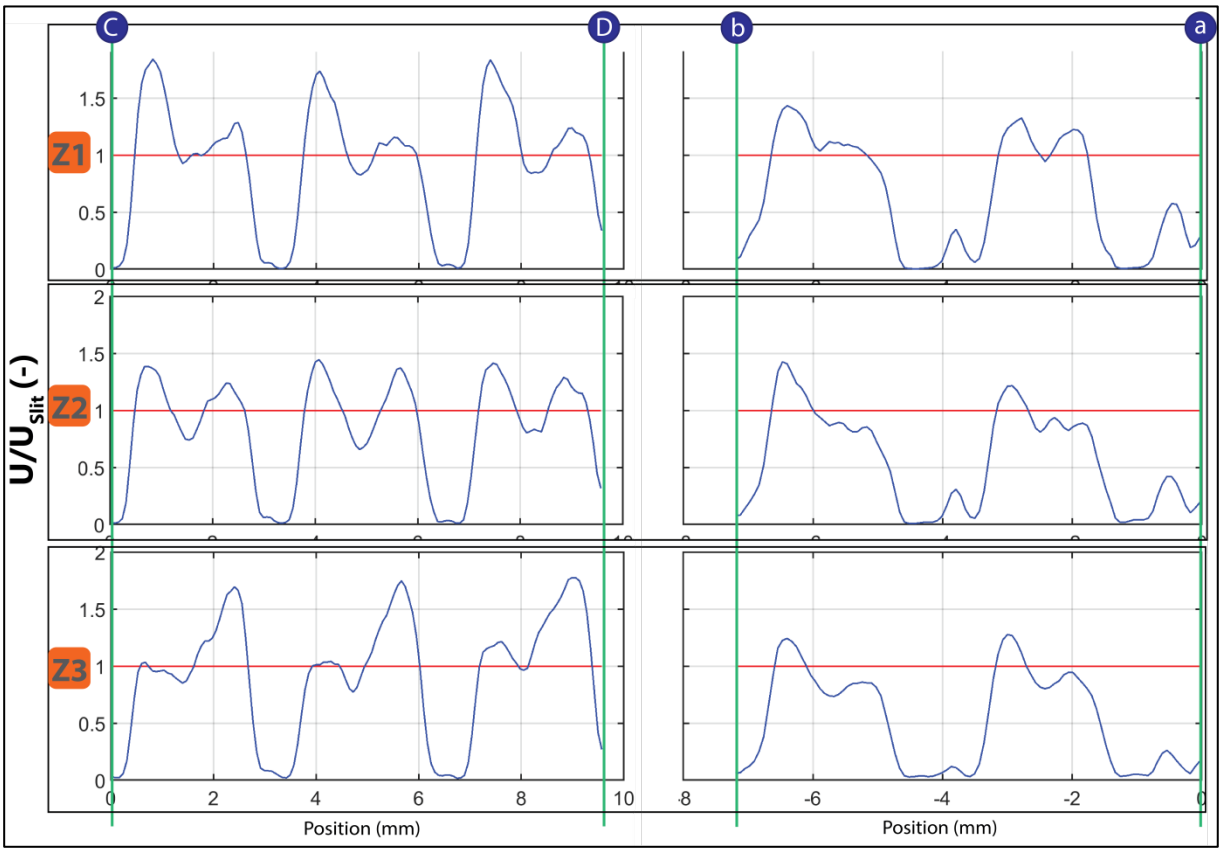

Figure 9: normalized velocity variation along a line in direction of the flow (line a-b) and perpendicular to the direction of the flow (line C-D) between two nodes of a spacer for planes Z1-Z3.

Temporal velocity pattern

The results from former section consider the effect of average inlet velocity on pressure drop and the variation of the velocity in place. In this section, we study the effect of time on the velocity in some specific points. Generally, a high velocity variation is preferred at a point, specifically a variation with a value above the specific average velocity. A high variation of velocity implies a local pulsation at a point and generation of pulsatile flow. This pulsatile flow contributes to fouling reduction, because

the amplitude shear oscillation is better than shear alone in minimization of fouling specially concentration polarization (Liang et al. 2016).

Figure 10 provides an overview of the temporal velocity for five points inside a mesh at three different heights (Z1, Z2, and Z3). The time interval between each measurement was in the range of milliseconds (Figure 4). The results shown here correspond to the average velocity values of 0.17m/s (Equation 1). Each box represents 50 measurements. The median, average and outliers are shown respectively with a straight line, empty circle inside the box and filled circles.

Figure 10 shows an unsteady characteristic of the flow in which the velocity varies over time at a particular point. The highest unsteadiness is observed in the middle of the mesh (E) and the lowest at downstream angle of the mesh (A) in all three levels. Also, the temporal velocity of where the water enters a mesh under a filament (point D) is higher compare to other points. In most cases, the unsteadiness at the membrane sides (Z1 and Z3) is slightly higher than the middle of the channel.

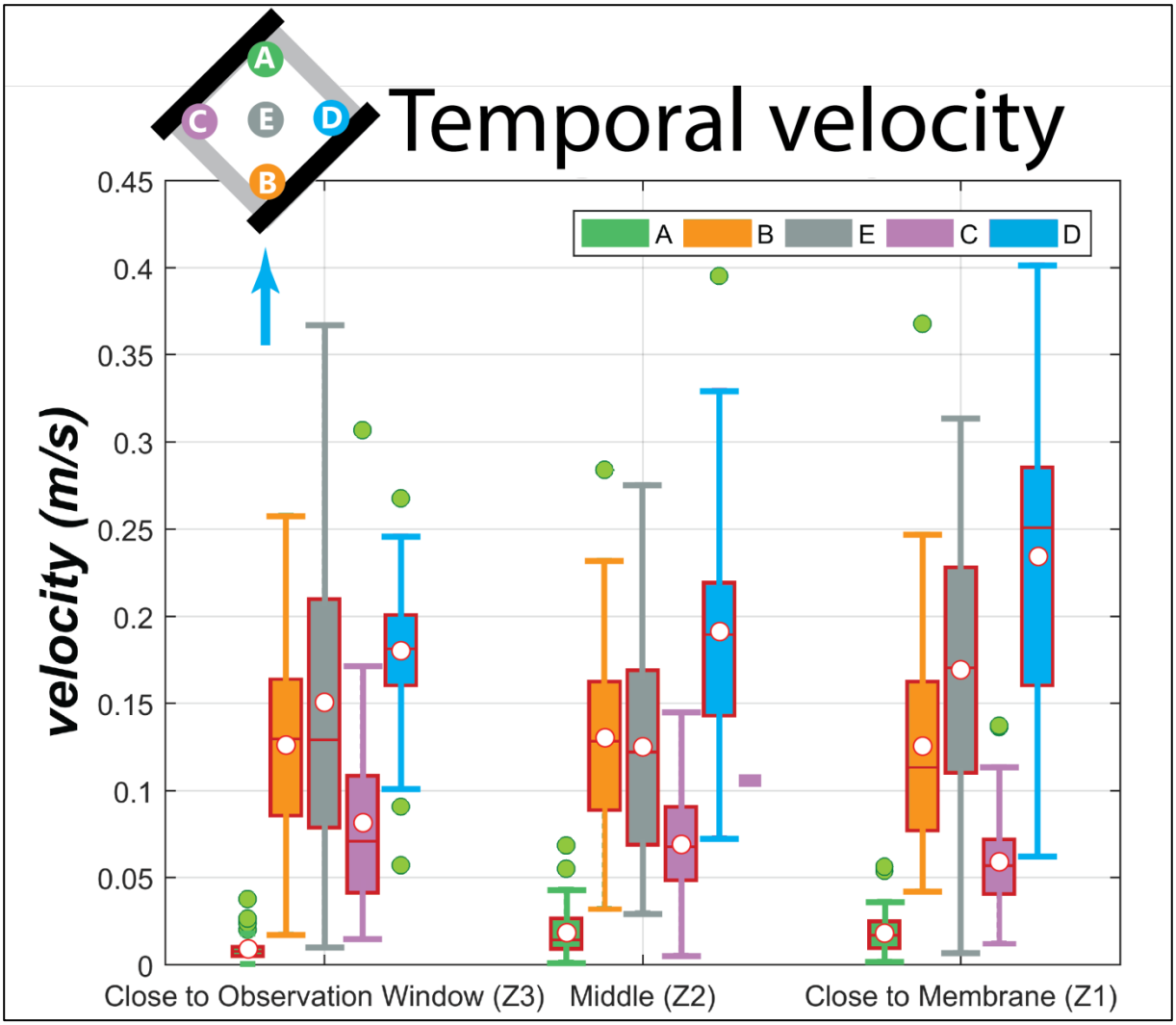

Figure 10: temporal velocity for empty (a) and spacer-filled (b) channel and the statistical comparison of these two scenarios (C).

Discussion

Many computation models are validated with experimental methods of much lower resolutions than the computational calculations itself. As shown in this work, PIV can provide detailed velocity profiles in empty and spacer-filled channels. Hence, such experimental information can be used as the input values for validation of computational models. Relating of the velocity pattern with the fouling can be used as tool for a better understanding of the fouling phenomena and improvement in the feed-spacer design in the future. For instance, the temporal and spatial velocity pattern in this study

shows that downstream of nodes (location such as point A in Figure 10) have high fouling potentials compare to the other places. The practical results show that such locations are places that particulate fouling occurs more intensively (Radu et al. 2014) than other places and the biofouling starts at such points. The initiation and development of biofouling at the nodes of the spacers is shown by different researchers (Ngene et al. 2010, Vrouwenvelder et al. 2010b).

This study is also illustrated the difference between the flow patterns in empty and spacer-filled channel. The velocity has statistically a shape of a unimodal and a bimodal normal distribution respectively in the empty and the spacer-filled channel (Figure 7). By increase of the inlet velocity as the results of increasing of the flow, the standard deviation of the velocity increases, which indicates a better mixing of the flow in xy-plane. A higher velocity at xy-plane is desirable for postponing of the fouling. However, this will be achieved by application of higher flow and consequently higher energy consumption. In this case, the pressure drops increases linearly in the empty channel and with a velocity power of about 1.74 for spacer with the same geometry as has described in this paper.

Conclusions

The temporal and the spatial velocity are investigated in the flat empty and the spacer-filled channel with the height of 0.76mm, which is a very common channel height in Spiral Wound (SW) modules of Reverse Osmosis (RO). The particle image velocimetry technique is used to obtain high resolution velocity maps and coated particles were used in combination with a cutoff filter to improve the quality of these vector maps. This paper gives information on the velocity pattern in the xy-plane and pressure drop over the length of the channel. The results achieved in this study showed agreement with previous numerical and experimental studies. Measurement of the velocity showed that there are low- and high-velocity zones inside each mesh. Some of these low-velocity zones, which also have low temporal velocity variations, are the places that deceleration of the particles happens and (bio)fouling initiates. The results from this study can provide information to validate computational

studies. The PIV-measurement for other configurations of the feed spacers reveals the effect of the spacers' geometry on the velocity pattern and the fouling potential of the feed spacers. Combining such measurement with the measurement of pressure drop and the results from the computational studies will lead to a better understanding of the hydraulic conditions in spacer-filled channel and consequently, design of the prefect spacer.

Acknowledgements

This research was made possible by the financial aid of Vitens Water Company. We also gratefully acknowledge the support provided by Dr. Cristian Picioreanu in the improvement of this article. We also like to thank Martin Verebes from DelStar Technologies inc. for providing us with the required feed spacers.

Nomenclature and abbreviations

d_f	Thickness of filament of spacer (m)
h_{sp}	Thickness of feed spacer (m)
H	Height of the feed channel (m)
l_m	Mesh length of spacer (m)
Q	Flow (m^3/s)
U_{eff}	Effective velocity (m/s)
Ux	Velocity in X-direction (velocity perpendicular to flow) (m/s)
W	Width (m)
Z1	XY-plane close to the membrane surface
Z2	XY-plane close to the middle of the feed channel at the boundary of top and bottom filaments
Z3	XY-plane close to Plexiglas surface
Greek symbols	
α	Flow attack angle
β	Hydrodynamic angle of feed spacer(^{o})
ε	Porosity of the feed spacer (-)

Abbreviation	
CFD	Computational fluid dynamics
FOV	Field Of View
PIV	Particle Image Velocimetry
RO	Reverse Osmosis
SW	Spiral Wound

Bibliography

Araùjo, P.A., Miller, D.J., Correia, P.B., van Loosdrecht, M.C.M., Kruithof, J.C., Freeman, B.D., Paul, D.R. and Vrouwenvelder, J.S. (2012) Impact of feed spacer and membrane modification by hydrophilic, bactericidal and biocidal coating on biofouling control. Desalination 295(0), 1-10.

Bucs, S.S., Radu, A.I., Lavric, V., Vrouwenvelder, J.S. and Picioreanu, C. (2014) Effect of different commercial feed spacers on biofouling of reverse osmosis membrane systems: A numerical study. Desalination 343, 26-37.

Da Costa, A.R. and Fane, A.G. (1994) Net-Type Spacers: Effect of Configuration on Fluid Flow Path and Ultrafiltration Flux, pp. 1845-1851, American Chemical Society.

Da Costa, A.R., Fane, A.G., Fell, C.J.D. and Franken, A.C.M. (1991) Optimal channel spacer design for ultrafiltration. Journal of Membrane Science 62(3), 275-291.

Da Costa, A.R., Fane, A.G. and Wiley, D.E. (1994) Spacer characterization and pressure drop modelling in spacer-filled channels for ultrafiltration. Journal of Membrane Science 87(1–2), 79-98.

Du Plessis, J. and Collins, M. (1992) A new definition for laminar flow entrance lengths of straight ducts. N&O Joernaal 25, 11-16.

Fimbres-Weihs, G.A. and Wiley, D.E. (2007) Numerical study of mass transfer in three-dimensional spacer-filled narrow channels with steady flow. Journal of Membrane Science 306(1–2), 228-243.

Fimbres-Weihs, G.A. and Wiley, D.E. (2010) Review of 3D CFD modeling of flow and mass transfer in narrow spacer-filled channels in membrane modules, pp. 759-781.

Gimmelshtein, M. and Semiat, R. (2005) Investigation of flow next to membrane walls. Journal of Membrane Science 264(1ΓÇô2), 137-150.

Klank, H., Goranović, G., Kutter, J.P., Gjelstrup, H., Michelsen, J. and Westergaard, C.H. (2002) PIV measurements in a microfluidic 3D-sheathing structure with three-dimensional flow behaviour. Journal of Micromechanics and Microengineering 12(6), 862.

Koutsou, C.P., Yiantsios, S.G. and Karabelas, A.J. (2007) Direct numerical simulation of flow in spacer-filled channels: Effect of spacer geometrical characteristics. Journal of Membrane Science 291(1ΓÇô2), 53-69.

Lau, K.K., Abu Bakar, M.Z., Ahmad, A.L. and Murugesan, T. (2009) Feed spacer mesh angle: 3D modeling, simulation and optimization based on unsteady hydrodynamic in spiral wound membrane channel. Journal of Membrane Science 343(1ΓÇô2), 16-33.

Li, F., Meindersma, W., de Haan, A.B. and Reith, T. (2002) Optimization of commercial net spacers in spiral wound membrane modules. Journal of Membrane Science 208(1ΓÇô2), 289-302.

Li, F., Meindersma, W., de Haan, A.B. and Reith, T. (2005) Novel spacers for mass transfer enhancement in membrane separations. Journal of Membrane Science 253(1ΓÇô2), 1-12.

Liang, Y.Y., Fimbres Weihs, G., Setiawan, R. and Wiley, D. (2016) CFD modelling of unsteady electro-osmotic permeate flux enhancement in membrane systems. Chemical Engineering Science 146, 189-198.

Neal, P.R., Li, H., Fane, A.G. and Wiley, D.E. (2003) The effect of filament orientation on critical flux and particle deposition in spacer-filled channels. Journal of Membrane Science 214(2), 165-178.

Ngene, I.S., Lammertink, R.G.H., Wessling, M. and Van der Meer, W.G.J. (2010) Particle deposition and biofilm formation on microstructured membranes. Journal of Membrane Science 364(1–2), 43-51.

Oberkampf, W.L. and Trucano, T.G. (2002) Verification and validation in computational fluid dynamics. Progress in Aerospace Sciences 38(3), 209-272.

Pellerin, E., Michelitsch, E., Darcovich, K., Lin, S. and Tam, C.M. (1995) Turbulent transport in membrane modules by CFD simulation in two dimensions. Journal of Membrane Science 100(2), 139-153.

Radu, A.I., van Steen, M.S.H., Vrouwenvelder, J.S., van Loosdrecht, M.C.M. and Picioreanu, C. (2014) Spacer geometry and particle deposition in spiral wound membrane feed channels. Water Research 64, 160-176.

Schausberger, P., Norazman, N., Li, H., Chen, V. and Friedl, A. (2009) Simulation of protein ultrafiltration using CFD: Comparison of concentration polarisation and fouling effects with filtration and protein adsorption experiments. Journal of Membrane Science 337(1–2), 1-8.

Schock, G. and Miquel, A. (1987) Mass transfer and pressure loss in spiral wound modules. Desalination 64(0), 339-352.

Schwinge, J., Neal, P.R., Wiley, D.E. and Fane, A.G. (2002) Estimation of foulant deposition across the leaf of a spiral-wound module. Desalination 146(1ΓÇô3), 203-208.

Thomas, D.G., Hayes, P.H., Mixon, W.R., Sheppard, J.D., Griffith, W.L. and Keller, R.M. (1970) Turbulence promoters for hyperfiltration with dynamic membranes, pp. 1129-1136, American Chemical Society.

Vrouwenvelder, J.S., Bakker, S.M., Wessels, L.P. and van Paassen, J.A.M. (2007) The Membrane Fouling Simulator as a new tool for biofouling control of spiral-wound membranes, pp. 170-174.

Vrouwenvelder, J.S., Buiter, J., Riviere, M., van der Meer, W.G.J., van Loosdrecht, M.C.M. and Kruithof, J.C. (2010a) Impact of flow regime on pressure drop increase and biomass accumulation and morphology in membrane systems. Water Research 44(3), 689-702.

Vrouwenvelder, J.S., Kappelhof, J.W.N.M., Heijrnan, S.G.J., Schippers, J.C. and van der Kooija, D. (2003) Tools for fouling diagnosis of NF and RO membranes and assessment of the fouling potential of feed water, pp. 361-365.

Vrouwenvelder, J.S., Manolarakis, S.A., van der Hoek, J.P., van Paassen, J.A.M., van der Meer, W.G.J., van Agtmaal, J.M.C., Prummel, H.D.M., Kruithof, J.C. and van Loosdrecht, M.C.M. (2008) Quantitative biofouling diagnosis in full scale nanofiltration and reverse osmosis installations. Water Research 42(19), 4856-4868.

Vrouwenvelder, J.S., Picioreanu, C., Kruithof, J.C. and van Loosdrecht, M.C.M. (2010b) Biofouling in spiral wound membrane systems: Three-dimensional CFD model based evaluation of experimental data. Journal of Membrane Science 346(1), 71-85.

Vrouwenvelder, J.S. and Van Der Kooij, D. (2003) Integral diagnosis of fouling problems by analysing biomass and inorganic compounds in membrane elements used in water treatment. Water science and technology: water supply, 211-215.

Vrouwenvelder, J.S., van Loosdrecht, M.C.M. and Kruithof, J.C. (2011) A novel scenario for biofouling control of spiral wound membrane systems. Water Research 45(13), 3890-3898.

Vrouwenvelder, J.S., van Paassen, J.A.M., van Agtmaal, J.M.C., van Loosdrecht, M.C.M. and Kruithof, J.C. (2009) A critical flux to avoid biofouling of spiral wound nanofiltration and reverse osmosis membranes: Fact or fiction? Journal of Membrane Science 326(1), 36-44.

Vrouwenvelder, J.S., van Paassen, J.A.M., Wessels, L.P., van Dam, A.F. and Bakker, S.M. (2006) The Membrane Fouling Simulator: A practical tool for fouling prediction and control. Journal of Membrane Science 281(1ΓÇô2), 316-324.

Willems, P., Deen, N.G., Kemperman, A.J.B., Lammertink, R.G.H., Wessling, M., van Sint Annaland, M., Kuipers, J.A.M. and van der Meer, W.G.J. (2010) Use of Particle Imaging Velocimetry to measure liquid velocity profiles in liquid and liquid/gas flows through spacer filled channels. Journal of Membrane Science 362(1ΓÇô2), 143-153.

Yee, K.W.K., Wiley, D.E. and Bao, J. (2009) A unified model of the time dependence of flux decline for the long-term ultrafiltration of whey. Journal of Membrane Science 332(1–2), 69-80.

Zimmerer, C.C. and Kottke, V. (1996) Effects of spacer geometry on pressure drop, mass transfer, mixing behavior, and residence time distribution. Desalination 104(1ΓÇô2), 129-134.